Skewed temperature dependence affects range and abundance in a warming world

Amy Hurford [1,2], Christina A. Cobbold [3], Péter K. Molnár [4,5]

[1]Department of Biology
[2]Department of Mathematics and Statistics
Memorial University
St. John's NL A1B 3X9, Canada
Tel: +1 709 864-8301
E-mail: ahurford@mun.ca

[3]School of Mathematics and Statistics
University of Glasgow,
University Place,
Glasgow, G12 8QS, UK
Tel: +44 141 330 4356
Fax: +44 141 330 4111
E-mail: christina.cobbold@glasgow.ac.uk

[4]Department of Biological Sciences
University of Toronto at Scarborough
1265 Military Trail
Toronto, Ontario, Canada M1C 1A4
Fax: 416-287-7676
Tel: +1 416-208-2247
Email: peter.molnar@utoronto.ca

[5]Department of Ecology and Evolutionary Biology, University of Toronto
25 Willcocks Street
Toronto, Ontario, Canada M5S 3B2

Abstract

Population growth metrics such as R_0 are usually asymmetric functions of temperature, with cold-skewed curves arising when the positive effects of a temperature increase outweigh the negative effects, and warm-skewed curves arising in the opposite case. Classically, cold-skewed curves are interpreted as more beneficial to a species under climate warming, because cold-skewness implies increased population growth over a larger proportion of the species' fundamental thermal niche than warm-skewness. However, inference based on the shape of the fitness curve alone, and without considering the synergistic effects of net reproduction, density, and dispersal may yield an incomplete understanding of climate change impacts. We formulate a moving-habitat integrodifference equation model to evaluate how fitness curve skewness affects species' range size and abundance during climate warming. In contrast to classic interpretations, we find that climate warming adversely affects populations with cold-skewed fitness curves, positively affects populations with warm-skewed curves and has relatively little or mixed effects on populations with symmetric curves. Our results highlight the necessity of considering the synergistic effects of fitness curve skewness, density, and dispersal in climate change impact analyses, and that the common approach of mapping changes only in R_0 may be misleading.

Keywords: climate change; integrodifference; Metabolic Theory; range shifts; thermal tolerance; niche

Introduction

Numerous species are undergoing range shifts in response to climate change, typically polewards in latitude or upwards in altitude[1–3]. Underlying these shifts are complex spatial dynamics that may include (i) regional extirpations in areas where conditions are becoming unsuitable, (ii) persistence, but with altered population dynamics in regions where conditions have changed but remain suitable, and (iii) dispersal, followed by potential establishment and growth, into regions where conditions have become newly suitable[4,5]. Depending on the respective strengths of these processes, the net effect may be an overall range contraction, a range shift, or a range expansion, as well as an overall decline or increase in abundance. Examples of such changes exist from almost all major taxa[1–3], including for some pathogens and pests, as well as for some species that provide ecosystem services[6–9].

One key element for determining the impacts of a warmer climate on a species' range and abundance is the temperature sensitivity of its population growth, which in turn is a consequence of the temperature sensitivities of the underlying life history components[10]. Mortality, for example, tends to increase exponentially with temperature within a species' thermal tolerance range, while fecundity in contrast exhibits a hump-shaped relationship – increasing first to some optimal temperature before decreasing again to zero at high temperatures (see [10] and references therein). In many insects and vertebrate ectotherms[10–12], these patterns combine to yield a unimodal, cold-skewed temperature-population growth relation that increases gradually to some optimum before dropping steeply to zero near the upper boundary of the species' tolerance range (Figure 1b). Environmentally transmitted nematode parasites, by contrast, can exhibit a warm-skewed population growth curve, because the mortality of free-living stages is directly affected by temperature, but reproduction – when occurring within an endotherm definitive host – is temperature-independent[13] (Figures 1c and 2b; see also ref. [14]). Intermediate cases also exist (i.e. more symmetric population growth curves in bacteria[15]; Figure 1d), and skewness may further vary between[16] and within taxa[17]. In general, fitness curves are expected to be cold-skewed when the positive effects of a temperature increase (e.g. increased reproduction) outweigh the negative effects (i.e. increased mortality), and are expected to be warm-skewed in the opposite case[18,19].

The shape of a species' temperature-dependent population growth curve has been highlighted as a key determinant of whether or where a species is likely to persist in a warming climate. For example, researchers often estimate a species' intrinsic rate of increase, r, or net reproductive number, R_0, as a function of temperature, and then evaluate whether population growth would increase or decrease in different locations under future climates[11,20–22], sometimes also comparing the total land area where increases are likely against the total area of likely decreases as a measure of the anticipated overall net climate change impact[21]. The logical consequence of this perspective is that species with a cold-skewed population growth curve should have an inherent advantage over species with a warm-skewed curve in a warming climate, because cold-skew maximizes the area over which population growth will increase in response to warming[7,18] (Figure 1b-d). This interpretation does not, however, explicitly consider the ability of a species to disperse into and colonize new habitats, nor does it account for potential population dynamics differences along the temperature gradients of a species' range. Here, we show that the explicit consideration of dispersal and population dynamics processes suggests the opposite interpretation, that is, that a warm-skewed population growth curve is more beneficial to a species under climate warming than a cold-skewed curve.

To explore how fitness curve skewness may affect a species' range size and abundance during climate change-induced range shifts, we formulate a moving-habitat[23] integrodifference equation (IDE) model that explicitly tracks population growth and dispersal along a thermally non-uniform shifting niche, and evaluates the transient and long-term spatiotemporal dynamics that emerge from these interacting processes. IDEs are particularly well-suited for describing the typical 'travelling wave' patterns of range expansions[24], and have been applied to invasive species, trees, and wildlife[25]. More recently, IDE models have also been formulated for situations where the niche itself is shifting due to climate change, showing how the speed of climate change, the size of a species' niche, as well as its population growth rate and dispersal ability interact to determine if a species will keep pace with its moving niche[26–28]. Such moving-habitat IDE models[26–28], and closely-related partial differential equation models[29,30], have, however, only considered vastly simplified representations of the temperature-dependence of population growth, typically assuming a constant, spatially uniform growth rate within the

niche, and a constant, spatially uniform decline rate elsewhere (but see [31]). Our model (i) accounts for temperature dependencies in reproduction and survival using relationships suggested by the Metabolic Theory of Ecology (MTE)[18,32], (ii) uses these relationships to formulate temperature-dependent population growth curves of varying degrees of skewness (Figure 2), (iii) uses numerical simulations to subject populations to climate change-induced habitat shifts, and (iv) evaluates how skewness affects range size, abundance, and the lags between the invasion front and the niche boundaries during climate change (Figure 1). Generally, we find that warming adversely affects populations with cold-skewed fitness curves, positively affects populations with warm-skewed fitness curves, has relatively little or mixed effects on populations with symmetric fitness curves, and that these results are largely robust against different choices of population growth and dispersal mechanisms.

Methods

IDE models describe the spatiotemporal dynamics of a population, treating space and time as continuous and discrete variables, respectively. The population density, $n_{t+1}(x)$, at location x in year $t+1$ is given by

$$n_{t+1}(x) = \int_{\Omega} f\big(n_t(y), T(y,t)\big) k(x-y)\, dy, \qquad (1)$$

where $f(n_t(y),T(y,t))$ describes the density- and temperature-dependent population growth at location y in year t, and the dispersal kernel $k(x\text{-}y)$ describes the probability of an individual dispersing from location y to location x after the population growth phase. Following population growth and dispersal, the integral totals the numbers of individuals arriving at location x from all possible origins (y in Ω), thus giving the new population density, $n_{t+1}(x)$. For simplicity, we model Ω as a one-dimensional domain [$-L,L$], corresponding to either a latitudinal temperature gradient from the equator to a pole, or to an elevation gradient from low to high. For convenience, but without loss of generality, we discuss our model for a latitudinal temperature gradient in the northern hemisphere, hereafter referring to $x=-L$ as the

"south" and $x=L$ as the "north" and assuming a linear temperature decrease from $y=-L$ to $y=L$ (Figure 1a).

For generality, we evaluate our model for compensatory (Beverton-Holt) and overcompensatory (Ricker) functions of population growth. Furthermore, we consider both exponentially bounded (Laplace) and fat-tailed (Cauchy) dispersal kernels to evaluate how climate warming effects on species range shifts may depend on the organisms' ability to disperse long distances (a larger proportion of the population disperses long distances with the Cauchy kernel than with the Laplace kernel[24]). In the main text, we focus our discussion of methods and results on the Beverton-Holt/Laplace scenario (Figures 3-4), and then evaluate the robustness of our conclusions to other combinations of growth and dispersal in the Supplementary Online Material (SOM Sections 3-5) summarizing these comparisons in Table 1.

The Laplace kernel for dispersal is given by

$$k(x-y) = \frac{1}{2D} exp\left(-\frac{1}{D}|x-y|\right), \tag{2}$$

and assumes that the probability of dispersal from location y to location x only depends on the distance $|x-y|$ with a mean dispersal distance D (see ref. [33] for a mechanistic derivation).

The Beverton-Holt model for population growth can be viewed as the discrete time analogue to the continuous time logistic equation, and is given by

$$f\big(n_t(y), T(y,t)\big) = \frac{R_0\big(T(y,t)\big)n_t(y)}{1+\left[\big(R_0\big(T(y,t)\big)-1\big)/K\right]n_t(y)}\ , \tag{3}$$

where K represents carrying capacity and $R_0(T)$ is the temperature-dependent net reproductive number, which we refer to as the 'fitness curve'. Both R_0 and K could be impacted by environmental conditions in multiple ways, but we focus only on temperature dependencies in the former to allow disentangling of the role of fitness curve shape on the range change dynamics without confounding these analyses via changes in habitat. We assume a fixed generation time of 1 year and describe the temperature dependence of population growth via the underlying temperature dependencies of fecundity and mortality,

$$R_0\big(T(y,t)\big) = \rho\big(T(y,t)\big)\sigma\big(T(y,t)\big), \tag{4}$$

where ρ is fecundity at low population density, σ is the annual survival probability at low population density, and $T(y,t)$ is temperature at location y at time t. For notational simplicity, we write $T(y,t)=T$ henceforth.

We describe the temperature sensitivities of both fecundity, $\rho(T)$, and survival, $\sigma(T)$, using relationships suggested by the Metabolic Theory of Ecology (MTE)[18,32]. Fecundity is typically cold-skewed, increasing exponentially with temperature within a species' fundamental thermal niche, and dropping steeply to zero near the upper and lower temperature boundaries of that range (Figure 2a). Assuming that this temperature dependency is largely driven by the temperature sensitivity of underlying metabolic processes, we use the Sharpe-Schoolfield model[18] to represent $\rho(T)$ and write

$$\rho(T) = \rho_0 e^{-\frac{E_\rho}{\kappa}\left(\frac{1}{T}-\frac{1}{T_0}\right)} \left(1 + e^{-\frac{E_\rho^L}{\kappa}\left(-\frac{1}{T}+\frac{1}{T_\rho^L}\right)} + e^{-\frac{E_\rho^H}{\kappa}\left(\frac{1}{T}-\frac{1}{T_\rho^H}\right)}\right)^{-1}, \tag{5}$$

where ρ_0 is the fecundity at a reference temperature T_0 (units: K), κ=8.62x10^{-5} eV K^{-1} is Boltzmann's constant, E_ρ is the average activation energy (units: eV) of the rate-limiting enzyme driving reproduction (determining the temperature sensitivity of fecundity at intermediate temperatures of the organism's niche), and E_ρ^L and E_ρ^H are the inactivation energies (units: eV) determining how abruptly fecundity drops to zero at the thermal tolerance boundaries.

Survival is typically also a unimodal function of temperature but, unlike fecundity, is usually warm-skewed, peaking near the lower boundary of the organism's fundamental niche and declining exponentially as temperatures increases (Figure 2b). As with fecundity, we use an MTE-based formulation[18] to capture these patterns, representing the temperature-dependent rate of mortality by

$$\mu(T) = \mu_0 e^{-\frac{E_\mu}{\kappa}\left(\frac{1}{T}-\frac{1}{T_0}\right)} \left(1 + e^{-\frac{E_\mu^L}{\kappa}\left(-\frac{1}{T}+\frac{1}{T_\mu^L}\right)} + e^{-\frac{E_\mu^H}{\kappa}\left(\frac{1}{T}-\frac{1}{T_\mu^H}\right)}\right), \tag{6}$$

and the proportion of individuals that survive one year by

$$\sigma(T) = \exp(-\mu(T)). \tag{7}$$

As with fecundity, the parameters E_μ, E_μ^L and E_μ^H determine the temperature sensitivity of mortality within and outside the lower and upper temperature thresholds, T_μ^L and T_μ^H, and T_0 is a reference temperature at which mortality equals μ_0.

To evaluate how the shape of the temperature-dependent fitness curve $R_0(T)$ (equation 4) influences the range change dynamics, we establish cold-skewed, warm-skewed, and symmetric $R_0(T)$ curves by assuming temperature sensitivities in fecundity only, mortality only, or both (Figure 2, cf. also ref. [18]) and by setting the inactivation energies such that they further accentuate the direction of any skew in $R_0(T)$ whilst ensuring that the fundamental niche is contained within the spatial domain (see SOM Section 1 for details). The magnitude of the skew is further manipulated in each of these cases by considering a biologically plausible range of activation energies[34] ($0.2 \leq E_\rho, E_\mu \leq 1.1$). We standardized each fitness curve so that the total reproductive potential of an organism across the entire landscape is always a constant. This calibration ensures that the shape of $R_0(T)$ is the main source of variation in all comparisons, and that qualitative differences in climate change impacts can therefore be attributed to differences in this fitness curve shape (SOM Section 2).

Model simulations and parameter values

We used computer simulations to explore the range change dynamics given by equations 1-7 when climate warming occurs. We allowed the population density to equilibrate before the onset of warming (at t=0), after which we increase the temperature at all locations by w=0.1°C yr^{-1} up until an increase of 10°C is achieved, and evaluate how warming alters a population's range size and abundance, as well as the lag between the northern boundary of the population range and of its thermal niche (see Figure 1e for definitions). Range size and abundance

191 changes are reported as percentage changes relative to the range and abundance at the onset
192 of warming (t=0), whereas lag is reported as the difference between future lags and the lag at
193 t=0 to facilitate comparisons between fitness curves with different shapes (see SOM Section 2.1
194 for details). The MATLAB code used to generate all simulations is provided on Figshare[35] (doi:
195 10.6084/m9.figshare.6955370) and further details of the simulation implementation are
196 available in the SOM (Sections 1 and 2).
197
198 **Results**
199 The numerical solutions of equations 1-7 with simulated climate warming reveal that the
200 species' distribution lags behind its shifting fundamental niche, a dynamic that is discussed in
201 detail in Svenning and Sandel (2013)[5]. We observe regions of 'colonization credit'[4], where
202 suitable habitat ($R_0(T)$>1) has yet to be fully colonized, and of 'extinction debt'[4,35], where
203 individuals continue to persist temporarily in unsuitable habitat ($R_0(T)$<1; Figure 3a-c; see
204 Figure 1e for definitions of colonization credit and extinction debt).
205 During climate warming, population density retains its general shape, but the skew of
206 $R_0(T)$ affects the length of habitat where the population is at carrying capacity (Figure 3a-f).
207 Populations with a warm-skewed $R_0(T)$ have small lags (Figures 3k and 4k) and small
208 colonization credits (Figure 3h), which means that most of the fundamental niche has been fully
209 colonized, and suggests increased range sizes (Figures 3k and 4e) and increased abundances
210 (Figures 3k and 4h) under climate warming. The opposite holds for cold-skewed $R_0(T)$, where a
211 larger lag (Figure 3j and 4j) results in large colonization credits (Figure 3g), meaning that a large
212 region of the fundamental niche has yet to be fully colonized, and leading to decreased range
213 sizes (Figures 3j and 4d) and decreased abundances (Figures 3j and 4g).
214 These differences in the range change dynamics of warm-skewed, symmetric, and cold-
215 skewed $R_0(T)$ can be understood by considering the population's potential for range expansions
216 at the leading range edge. Populations with warm-skewed $R_0(T)$ are sensitive to beneficial
217 temperature increases in the north, where the slope of the $R_0(T)$ curve is steep. In addition,
218 warm-skewed populations have higher densities at the leading edge of their fundamental niche
219 (Figure 3b) due to smaller lags (Figure 4k), and thus a large potential for colonizing newly

available northern habitats via dispersal, resulting in an increased range size and abundance during warming (Figure 4e,h). For populations with a cold-skewed $R_0(T)$, these same mechanisms act in the opposite direction, implying decreased range sizes and abundance. Extinctions at the trailing edge of the population density also determine the net impact of climate warming, but the extinction debt is similar for $R_0(T)$ of all skewnesses (Figures 3g-i and S2). Populations with a symmetric $R_0(T)$ are mostly unaffected by climate warming, but demonstrate slight decreases in both range size and abundance (Figure 4f,i). These slight decreases occur where the population lags behind its fundamental niche, resulting in a negative net effect of colonization versus extinction, despite the symmetry of $R_0(T)$.

In contrast to the suggestion by Molnár *et al.* (2013)[18] that cold-skewed populations experience increased population growth over the majority of their habitat (orange bars in Figure 1b) and warm-skewed populations experience increased growth over only a small portion of their habitat (orange bars in Figure 1c), we find that generally climate warming adversely affects the range size, abundance and lag of populations with a cold-skewed $R_0(T)$, positively affects populations with a warm-skewed $R_0(T)$, and has relatively little or mixed effects on populations with a symmetric $R_0(T)$ (Figure 4; Table 1). For cold- and warm-skewed $R_0(T)$, the degree of the skew further magnifies these effects. This result is a consequence of the interaction between population growth, density, and dispersal, which is masked when one considers population growth in isolation as a predictor of climate warming affects.

The influence of $R_0(T)$'s skewness on a population's response to climate warming is largely insensitive to mean dispersal distance, the choice of population growth function, and the choice for dispersal kernel (SOM Sections 3-5; summarized in Table 1). Using an overcompensatory population growth function (Ricker) instead of the compensatory Beverton-Holt function generally yields final ranges, abundances and lags that are similar to those outlined for the Beverton-Holt scenario (Table 1; SOM Section 3). However, for large values of $R_0(T)$, Ricker growth may give rise to oscillatory or chaotic travelling waves that do not occur with Beverton-Holt growth[26], and it is noteworthy that these oscillations can be dampened by climate warming due to the temperature dependence of $R_0(T)$ (SOM Section 4). Using a fat-

248 tailed (Cauchy) dispersal kernel instead of the Laplace kernel yields some minor differences, but
249 our general results remain qualitatively unaffected (Table 1; SOM Section 5).
250
251 **Discussion**
252 The shape of temperature-dependent population growth measures such as $R_0(T)$ contains
253 critical information on a species' sensitivity to climate change. The common approach of only
254 considering how population growth metrics such as $R_0(T)$ or $r(T)$ would change in different
255 locations under climate change (e.g. $R_0(T)$- or $r(T)$-based impact maps for insects[11], wildlife
256 pathogens[22], and human pathogens[20,21]), however, can yield an incomplete and potentially
257 misleading picture. Cold-skewed $R_0(T)$ have previously been interpreted as more beneficial to
258 species' persistence under warming because cold-skewness implies fitness increases over a
259 comparatively larger portion of habitat[7,18] (Figure 1b-d). Explicit consideration of the population
260 growth-dispersal dynamics in our moving-habitat IDE framework, however, revealed that
261 species with a cold-skewed $R_0(T)$ may in fact be more likely to experience adverse impacts
262 during warming than species with a warm-skewed $R_0(T)$. With a warm-skewed $R_0(T)$ steep
263 fitness increases and relatively large densities at the northern range limit allow for rapid
264 abundance increases in areas that have not yet been fully colonized, while more gradual fitness
265 declines combined with smaller densities simultaneously limit the extinction risk at the trailing
266 niche edge. The opposite is true for species with cold-skewed $R_0(T)$. It is these synergistic effects
267 of $R_0(T)$ skewness, spatially varying population densities, and dispersal that underly our findings
268 that a warm-skewed $R_0(T)$ results in range size and abundance increases and small lags between
269 the moving leading edge of the fundamental niche and the population's range edge, whereas a
270 cold-skewed $R_0(T)$ results in range contractions, decreased abundances, and large lags.
271 Our model is deliberately simple to facilitate a sound understanding of the key
272 processes determining range changes (dispersal, fecundity, and mortality). It is intended for
273 separating out the influence of fitness curve skewness arising from imbalances in the
274 temperature sensitivity of life history components (here, fecundity and mortality) from multiple
275 other factors that may also influence range change dynamics. Our analyses highlight the
276 synergistic effects of fitness curve skewness, density, and dispersal as a previously unrecognized

277 mechanism for why some species may benefit from warming while others experience range
278 contractions and population declines, but these mechanisms should be viewed as
279 complementary to previously recognized influences, such as the role of interspecific
280 interactions[38] or dispersal limitation[39] in confining species to only part of their fundamental
281 niche.

282 The muskox lungworm *Umingmakstrongyls pallikuukensis*, for example, has a warm-
283 skewed $R_0(T)$[13] and has been closely tracking the northern boundary of its shifting fundamental
284 niche during a warming-induced range expansion[6] as would be expected (Figures 3-4). No
285 changes were reported in the southern boundary of the lungworm's distribution[6], which is
286 consistent with our results that warm-skewed $R_0(T)$ still have large extinction debts (Figure 3h),
287 and may further be explained by the worm benefitting from the behavioral thermoregulation of
288 its intermediate slug host and the shelter it provides from lethal high-temperature extremes[13].
289 Also in agreement with our results are the range contractions observed in tree species in the
290 eastern United States[40] and southern Africa[41], where limited dispersal resulted in large
291 dispersal lags at the poleward limits, perhaps further exacerbated by apparently cold-skewed
292 fitness curves (cf. Figure 3 in Talluto et al.[4]). Lepidopterans[8,9] and Odonata[42], by contrast, have
293 largely expanded their ranges polewards in response to warming – often while maintaining
294 stable or more slowly moving equatorward boundaries – despite generally cold-skewed fitness
295 curves (see Deutsch et al. 2008[11], their Dataset S1). It has, however, been suggested that these
296 range change patterns could be a result of temperature limiting species' distribution at the
297 poleward boundary, and factors other than temperature (e.g. competition) currently limiting
298 distribution at the equatorward boundary[8,9,42]. In other words, these species may not be fully
299 occupying the warmest end of their fundamental thermal niche, and would thus temporarily be
300 shielded from the worst consequences of warming despite having a cold-skewed fitness curve.

301 The dynamics of climate warming-induced range changes are complex and our analyses
302 are not meant to imply that skewness will uniquely determine whether warming benefits or
303 harms a species. Dedicated meta-analyses are needed to disentangle the various factors
304 affecting range changes (i.e., dispersal limitation[39], sensitivities to other abiotic variables[43],
305 biotic interactions[44], and landscape features[45,46]), but are currently limited by (i) unknown

306 fitness curve shapes for most species, (ii) the difficulty of inferring fitness curve shape from
307 local densities when carrying capacity is temperature-independent as assumed here (cf. Figure
308 3a-f, showing 'rectangular travelling waves with soft edges' regardless of fitness curve skew),
309 and (iii) a paucity of studies[47] documenting distribution and abundance changes over a species'
310 entire range and on long-enough time scales to capture the dynamics suggested here.
311 Nevertheless, given the robustness of our results to different forms of density dependence and
312 dispersal (Table 1), we expect that imbalances in the temperature sensitivities of different life
313 history traits and the resultant fitness curve skewness may explain some of the observed
314 variation in distribution and abundance change responses to climate warming.

315 Our models can be easily extended in multiple ways by relaxing simplifying assumptions
316 or adding additional population regulating mechanisms. The list of potential factors influencing
317 range change dynamics is long, and includes potential temperature dependencies in other life
318 history components (i.e. increased temperature would imply: decreased carrying capacity, since
319 faster metabolism accelerates the depletion of a fixed resource supply[12]; decreased
320 development times, due to faster metabolism[32]; and shortened dispersal distances in marine
321 plankton[48], due to decreased larval development time[32]), local adaptation (e.g. different
322 temperature sensitivities of individuals at the leading and trailing edge[17]), environmental
323 stochasticity (e.g. influencing individuals at the cold and warm ends of their range differently
324 due to Jensen's inequality[49–51]), limiting abiotic factors other than temperature[43] (e.g.
325 moisture), age-structure[27] (e.g. for species where dispersal only occurs in certain life stages
326 such as trees or many insects), Allee effects limiting range shift speeds at the leading edge[24,25],
327 as well as landscape heterogeneities[45,46], or species interactions[29,38,44]. Each of these might
328 dampen or amplify the patterns suggested by our analyses.

329 We used temperature-dependent relationships only for fecundity and survival but did
330 not explore the effects of temperature dependence on generation time. This assumption most
331 closely corresponds to organisms with a fixed, one-year generation, for example driven by
332 obligatory diapause to overwinter a cold season (e.g. Lepidoptera in temperate forests).
333 However, even in these cases, generation time may decrease if development increases
334 sufficiently fast with increasing temperatures to allow for multiple generations within a year.

Such changes would not affect $R_0(T)$ (because it measures population growth per generation)[10,52], but would shift the relationship between temperature and the intrinsic rate of population growth increase, $r(T)$, towards more cold-skewed, likely with the corresponding consequences for abundance and range changes that were outlined above. Our combined MTE-IDE framework allows easy incorporation of such additional factors.

The MTE describes temperature effects from the individual to the ecosystem level[32] and has provided many insights on how a warmer climate may alter population and community dynamics[18,34,46,53], but analyses have generally been limited to non-spatial effects to date. Likewise, there exists a rich literature that uses integrodifference equation models to explore how various intrinsic and extrinsic mechanisms[24,25,27,33,45,46] affect range change dynamics, but few studies have explicitly explored the role of temperature in these dynamics. Combining these two bodies of theory has enormous potential for unravelling the complexities of temperature-dependent spatial population dynamics.

Acknowledgements

This research was catalyzed by a Banff International Research Station workshop (13w5095) and further facilitated by an Atlantic Association for Research in the Mathematical Sciences Collaborative Research Grant. AH (RGPIN 2014-05413) and PKM (RGPIN 2016-06301) were supported by National Sciences and Engineering Research Council of Canada Discovery grants, and PKM was further supported by the Canada Foundation for Innovation John R. Evans Leader Funds, and MRIS Ontario Research Funds. CC was supported by the Biotechnology and Biological Sciences Research Council (BB/P004202/1). Part of this work was carried out while CC was a funded visiting scholar at the Fields Institute for Research in Mathematical Sciences.

References

1. Walther, G.-R. *et al.* Ecological responses to recent climate change. *Nature* **416,** 389–395 (2002).
2. Chen, I.-C., Hill, J. K., Ohlemueller, R., Roy, D. B. & Thomas, C. D. Rapid Range Shifts of Species Associated with High Levels of Climate Warming. *Science* **333,** 1024–1026 (2011).

3. Parmesan, C. & Yohe, G. A globally coherent fingerprint of climate change impacts across natural systems. *Nature* **421,** 37–42 (2003).
4. Talluto, M. V., Boulangeat, I., Vissault, S., Thuiller, W. & Gravel, D. Extinction debt and colonization credit delay range shifts of eastern North American trees. *Nat. Ecol. Evol.* **1,** s41559–017–0182–017 (2017).
5. Svenning, J.-C. & Sandel, B. Disequilibrium Vegetation Dynamics Under Future Climate Change. *Am. J. Bot.* **100,** 1266–1286 (2013).
6. Kutz, S. J. *et al.* Invasion, establishment, and range expansion of two parasitic nematodes in the Canadian Arctic. *Glob. Change Biol.* **19,** 3254–3262 (2013).
7. Altizer, S., Ostfeld, R. S., Johnson, P. T. J., Kutz, S. & Harvell, C. D. Climate change and infectious diseases: from evidence to a predictive framework. *Science* **341,** 514–519 (2013).
8. Parmesan, C. *et al.* Poleward shifts in geographical ranges of butterfly species associated with regional warming. *Nature* **399,** 579–583 (1999).
9. Chen, I.-C. *et al.* Asymmetric boundary shifts of tropical montane Lepidoptera over four decades of climate warming. *Glob. Ecol. Biogeogr.* **20,** 34–45 (2011).
10. Amarasekare, P. & Savage, V. A framework for elucidating the temperature dependence of fitness. *Am. Nat.* **179,** 178–191 (2012).
11. Deutsch, C. A. *et al.* Impacts of climate warming on terrestrial ectotherms across latitude. *Proc. Natl. Acad. Sci.* **105,** 6668–6672 (2008).
12. Savage, V. M., Gilloly, J. F., Brown, J. H. & Charnov, E. L. Effects of body size and temperature on population growth. *Am. Nat.* **163,** 429–441 (2004).
13. Molnár Péter K., Dobson Andrew P. & Kutz Susan J. Gimme shelter – the relative sensitivity of parasitic nematodes with direct and indirect life cycles to climate change. *Glob. Change Biol.* **19,** 3291–3305 (2013).

388 14. Gehman, A.-L. M., Hall, R. J. & Byers, J. E. Host and parasite thermal ecology jointly determine the
389 effect of climate warming on epidemic dynamics. *Proc. Natl. Acad. Sci. U. S. A.* **115,** 744–749
390 (2018).
391 15. Ratkowsky, D. A., Olley, J., McMeekin, T. A. & Ball, A. Relationship between temperature and
392 growth rate of bacterial cultures. *J. Bacteriol.* **149,** 1–5 (1982).
393 16. Ehnes Roswitha B., Rall Björn C. & Brose Ulrich. Phylogenetic grouping, curvature and
394 metabolic scaling in terrestrial invertebrates. *Ecol. Lett.* **14,** 993–1000 (2011).
395 17. Sunday, J. M., Bates, A. E. & Dulvy, N. K. Global analysis of thermal tolerance and latitude in
396 ectotherms. *Proc. R. Soc. Lond. B Biol. Sci.* rspb20101295 (2010). doi:10.1098/rspb.2010.1295
397 18. Molnár, P. K., Kutz, S. J., Hoar, B. M. & Dobson, A. P. Metabolic approaches to understanding
398 climate change impacts on seasonal host-macroparasite dynamics. *Ecol. Lett.* **16,** 9–21 (2013).
399 19. Molnár, P. K., Sckrabulis, J. P., Altman, K. A. & Raffel, T. R. Thermal performance curves and the
400 metabolic theory of ecology - a practical guide to models and experiments for parasitologists. *J.*
401 *Parasitol.* (2017). doi:10.1645/16-148
402 20. Ogden, N. H. *et al.* Estimated effects of projected climate change on the basic reproductive
403 number of the Lyme disease vector Ixodes scapularis. *Environ. Health Perspect.* **122,** 631–638
404 (2014).
405 21. Ryan, S. J. *et al.* Mapping Physiological Suitability Limits for Malaria in Africa Under Climate
406 Change. *Vector Borne Zoonotic Dis. Larchmt. N* **15,** 718–725 (2015).
407 22. Rose, H. *et al.* Climate-driven changes to the spatio-temporal distribution of the parasitic
408 nematode, Haemonchus contortus, in sheep in Europe. *Glob. Change Biol.* **22,** 1271–1285
409 (2016).
410 23. Harsch, M. A. *et al.* Moving forward: insights and applications of moving-habitat models for
411 climate change ecology. *J. Ecol.* **105,** 1169–1181 (2017).

24. Kot, M., Lewis, M. A. & van den Driessche, P. Dispersal Data and the Spread of Invading Organisms. *Ecology* **77,** 2027–2042 (1996).

25. Hastings, A. *et al.* The spatial spread of invasions: new developments in theory and evidence. *Ecol. Lett.* **8,** 91–101 (2005).

26. Zhou, Y. & Kot, M. Discrete-time growth-dispersal models with shifting species ranges. *Theor. Ecol.* **4,** 13–25 (2011).

27. Harsch, M. A., Zhou, Y., HilleRisLambers, J. & Kot, M. Keeping pace with climate change: stage-structured moving-habitat models. *Am. Nat.* **184,** 25–37 (2014).

28. Harsch, M. A. *et al.* Moving forward: insights and applications of moving-habitat models for climate change ecology. *J. Ecol.* **105,** 1169–1181 (2017).

29. Potapov, A. B. & Lewis, M. A. Climate and competition: the effect of moving range boundaries on habitat invasibility. *Bull. Math. Biol.* **66,** 975–1008 (2004).

30. Berestycki, H., Diekmann, O., Nagelkerke, C. J. & Zegeling, P. A. Can a species keep pace with a shifting climate? *Bull. Math. Biol.* **71,** 399–429 (2009).

31. Zhou, Y. in *Geographic range shifts under climate warming* (PhD thesis. University of Washingtion, 2013).

32. Brown, J. H., Gillooly, J. F., Allen, A. P., Savage, V. M. & West, G. B. Toward a metabolic theory of ecology. *Ecology* **85,** 1771–1789 (2004).

33. Neubert, M. G., Kot, M. & Lewis, M. A. Dispersal and Pattern Formation in a Discrete-Time Predator-Prey Model. *Theor. Popul. Biol.* **48,** 7–43 (1995).

34. Dell, A. I., Pawar, S. & Savage, V. M. Systematic variation in the temperature dependence of physiological and ecological traits. *Proc. Natl. Acad. Sci.* **108,** 10591–10596 (2011).

35. Hurford, A., Cobbold, C. A. & Molnár, P. Skewed temperature dependence affects range and abundance in a warming world (Code). (2018).

36. Tilman, D., May, R. M., Lehman, C. L. & Nowak, M. A. Habitat destruction and the extinction debt. *Nature* **371,** 65–66 (1994).

37. Kot, M. & Schaffer, W. M. Discrete-time growth-dispersal models. *Math. Biosci.* **80,** 109–136 (1986).

38. Ettinger, A. K. & HilleRisLambers, J. Climate Isn't Everything: Competitive Interactions and Variation by Life Stage Will Also Affect Range Shifts in a Warming World. *Am. J. Bot.* **100,** 1344–1355 (2013).

39. Brown, C. D. *et al.* Reproduction as a bottleneck to treeline advance across the circumarctic forest tundra ecotone. *Ecography* **0,**

40. Zhu, K., Woodall, C. W. & Clark, J. S. Failure to migrate: lack of tree range expansion in response to climate change. *Glob. Change Biol.* **18,** 1042–1052 (2012).

41. Foden, W. *et al.* A changing climate is eroding the geographical range of the Namib Desert tree Aloe through population declines and dispersal lags. *Divers. Distrib.* **13,** 645–653 (2007).

42. Hickling, R., Roy, D. B., Hill, J. K. & Thomas, C. D. A northward shift of range margins in British Odonata. *Glob. Change Biol.* **11,** 502–506 (2005).

43. Tingley, M. W., Koo, M. S., Moritz, C., Rush, A. C. & Beissinger, S. R. The push and pull of climate change causes heterogeneous shifts in avian elevational ranges. *Glob. Change Biol.* **18,** 3279–3290 (2012).

44. Brooker, R. W., Travis, J. M. J., Clark, E. J. & Dytham, C. Modelling species' range shifts in a changing climate: The impacts of biotic interactions, dispersal distance and the rate of climate change. *J. Theor. Biol.* **245,** 59–65 (2007).

45. Dewhirst, S. & Lutscher, F. Dispersal in heterogeneous habitats: thresholds, spatial scales, and approximate rates of spread. *Ecology* **90,** 1338–1345 (2009).

46. Gilbert, M. A., White, S. M., Bullock, J. M. & Gaffney, E. A. Spreading speeds for stage structured plant populations in fragmented landscapes. *J. Theor. Biol.* **349,** 135–149 (2014).

461 47. Lenoir, J. & Svenning, J.-C. Climate-related range shifts – a global multidimensional synthesis
462 and new research directions. *Ecography* **38,** 15–28
463 48. O'Connor, M. I. *et al.* Temperature control of larval dispersal and the implications for marine
464 ecology, evolution, and conservation. *Proc. Natl. Acad. Sci. U. S. A.* **104,** 1266–1271 (2007).
465 49. Estay, S. A., Lima, M. & Bozinovic, F. The role of temperature variability on insect performance
466 and population dynamics in a warming world. *Oikos* **123,** 131–140 (2014).
467 50. Ruel, J. J. & Ayres, M. P. Jensen's inequality predicts effects of environmental variation. *Trends*
468 *Ecol. Evol.* **14,** 361–366 (1999).
469 51. Vasseur, D. A. *et al.* Increased temperature variation poses a greater risk to species than climate
470 warming. *Proc. R. Soc. Lond. B Biol. Sci.* **281,** 20132612 (2014).
471 52. Huey, R. B. & Berrigan, D. Temperature, demography, and ectotherm fitness. *Am. Nat.* **158,** 204–
472 210 (2001).
473 53. O'Connor, M. I., Gilbert, B. & Brown, C. J. Theoretical predictions for how temperature affects the
474 dynamics of interacting herbivores and plants. *Am. Nat.* **178,** 626–638 (2011).
475
476

Table 1. The skewness of $R_0(T)$ has a strong influence on a population's response to climate warming, and these effects are insensitive to different choices for the population growth function, the dispersal kernel, and the mean dispersal distance. In response to 100 years of warming, ranges and abundances generally decrease (-) with a cold-skewed $R_0(T)$, increase (+) with a warm-skewed $R_0(T)$, and remain relatively unchanged (0) with a symmetric $R_0(T)$ in all cases except when a Cauchy kernel is used for dispersal (Cases 3-4).

Scenario	Population metric	Response after 100 years of climate warming			Additional information
		Cold skew	Warm skew	Symm.	
Case 1 • Beverton-Holt • Laplace	Range	-	+	0	Results are insensitive to variation in mean dispersal distance, *D* (equation 2), Figures S2 and S3.
	Abundance	-	+	0	
Case 2 • Ricker • Laplace	Range	-	+	0	Results are indistinguishable from Case 1 for small values of $R_0(T)$ (Figures S4 and S5). For large values of $R_0(T)$, population cycles may appear and climate change influences the amplitude of these cycles (Figure S6).
	Abundance	-	+	0	
Case 3 • Beverton-Holt • Cauchy	Range	0	+	+	Figures S5 and S7.
	Abundance	-	+	-	
Case 4 • Ricker • Cauchy	Range	0	+	+	Figure S5
	Abundance	-	+	0	

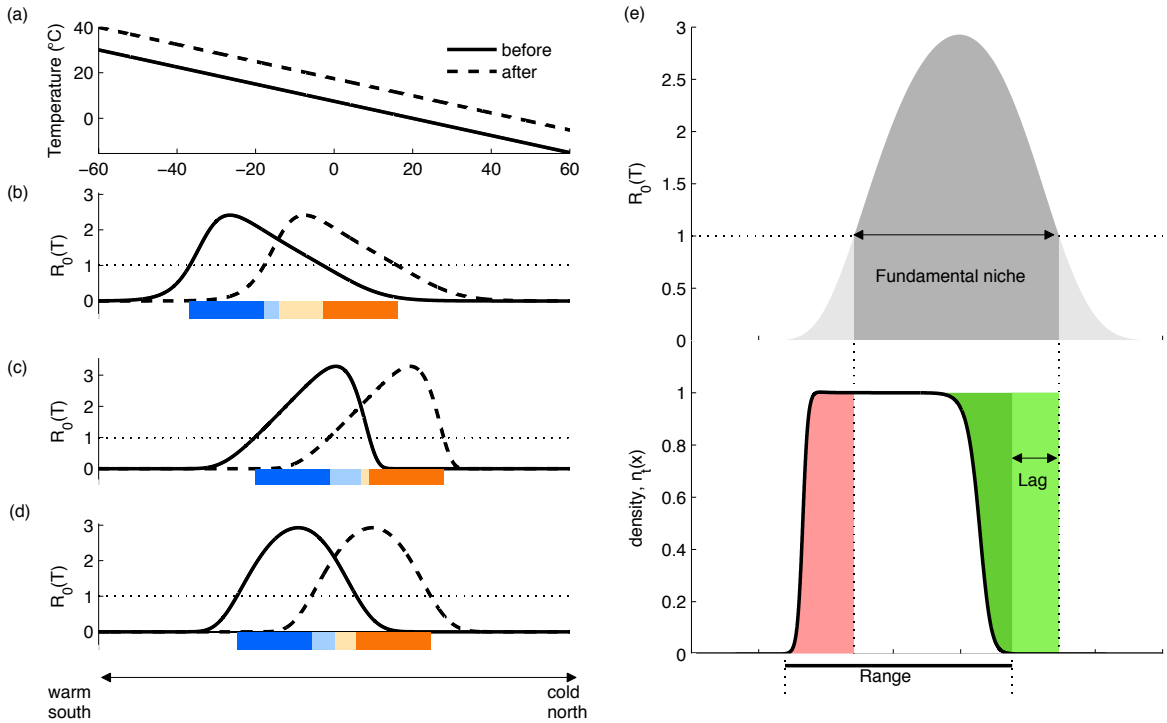

Figure 1. Summary statistics used to quantify the impacts of climate warming in model simulations. In the left column, panel (a) illustrates the hypothetical south-to-north temperature gradient before and after climate warming. The panels immediately below show $R_0(T)$ at corresponding spatial locations for (b) cold-skewed, (c) warm-skewed, and (d) symmetric $R_0(T)$. In all panels, solid lines refer to pre-warming baseline temperatures, and dashed lines to an environment that is 10°C warmer at each location. With warming, the $R_0(T)$ fitness curve shifts northwards, leading to increased fitness at northern locations (areas marked orange), allowing for a potential range expansion into newly suitable areas (regions where $R_0(T)>1$ after climate warming, but $R_0(T)<1$ before warming; dark orange); simultaneously, fitness decreases at southern locations (blue), extirpating the population from areas that have become too warm (regions where $R_0(T)<1$ after warming, but $R_0(T)>1$ before warming; dark blue). The percentage of the color bar that is orange is the percentage of the habitat that has exhibited increased growth, but excluding the regions that are unsuitable both before and after climate warming (cold-skewed: 57%, warmed-skewed: 44%, symmetric: 50%); illustrating the classic argument that, without explicit consideration of dispersal and population growth, populations with cold-skewed fitness curves are expected to perform better under warming than populations with symmetric or warm-skewed curves[7,18]. In the right column, panel (e) illustrates the 'fundamental thermal niche', defined as the locations where $R_0(T)>1$, as well as the summary metrics: ‘range’, ‘abundance’, ‘lag’, ‘extinction debt’ and ‘colonization credit’. The length of the spatial domain where the population density is above 0.001 defines the 'range'. The numerical integral of the population densities across the spatial domain defines the ‘abundance’. The distance between the location of the front of the range and the front of the fundamental niche defines the 'lag' (light green). 'Extinction debt', (pink) is the size of the population in locations where the population is present but eventually expected to become

extirpated due to $R_0(T)$<1; 'colonization credit' (green) is the difference between present density and the carrying capacity where the population could persist following future colonization due to $R_0(T)$>1.

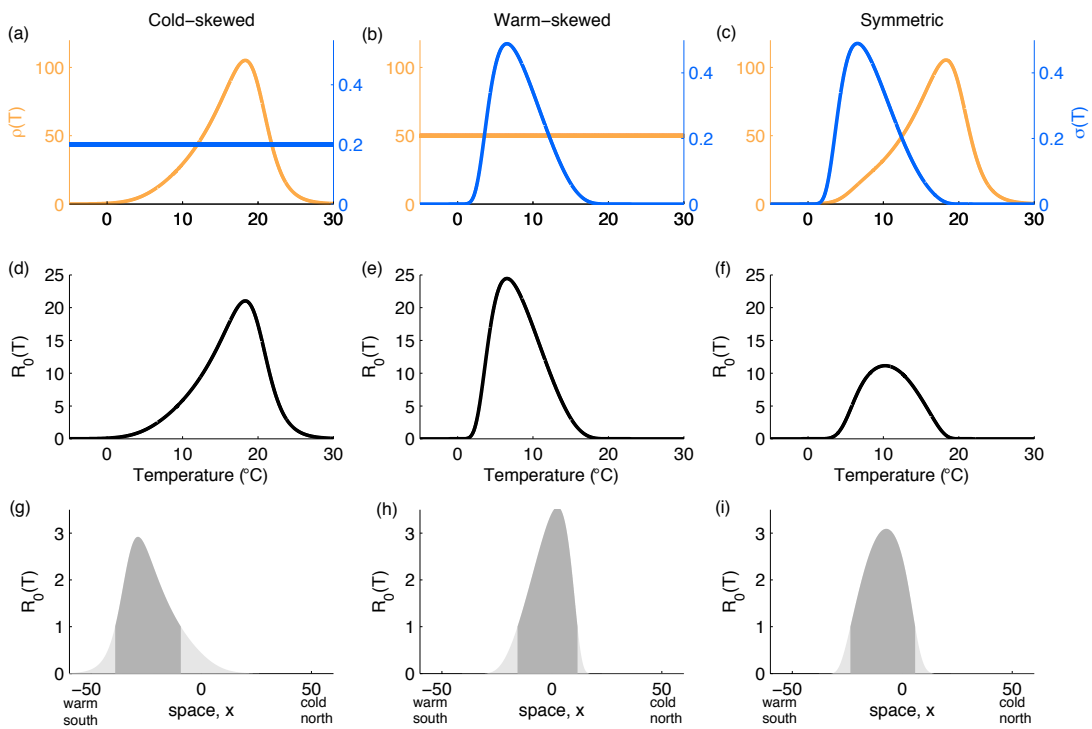

Figure 2. Temperature dependence in fecundity only, survival only, or both fecundity and survival yields $R_0(T)$ curves with different directions of skew. (a-c) Sharpe-Schoolfield equations (equations 5-7) describe the temperature dependence of fecundity ($\rho(T)$, orange) and survival ($\sigma(T)$, blue), yielding (d-f) the temperature-dependent $R_0(T)$ as the product of these two quantities (equation 4), and (g-i) the spatial dependence of R_0 by combining $R_0(T)$ with a spatial temperature gradient (here, linearly decreasing from 30°C at x=-60 in the south to -15°C at x=60 in the north). In the left column only fecundity depends on temperature with $E_\rho^L = 3$ eV, $E_\rho^H = 6$ eV, and $\mu(T)=\mu_0=-\ln(0.2)$. In the middle column only survival depends on temperature with E_μ^L=6 eV, E_μ^H=3 eV, and $\rho(T) = \rho_0 = 50$. In the right column both fecundity and survival are temperature-dependent with $E_\rho^L = E_\rho^H = E_\mu^L = E_\mu^H = 5E_\rho = 5E_\mu$.

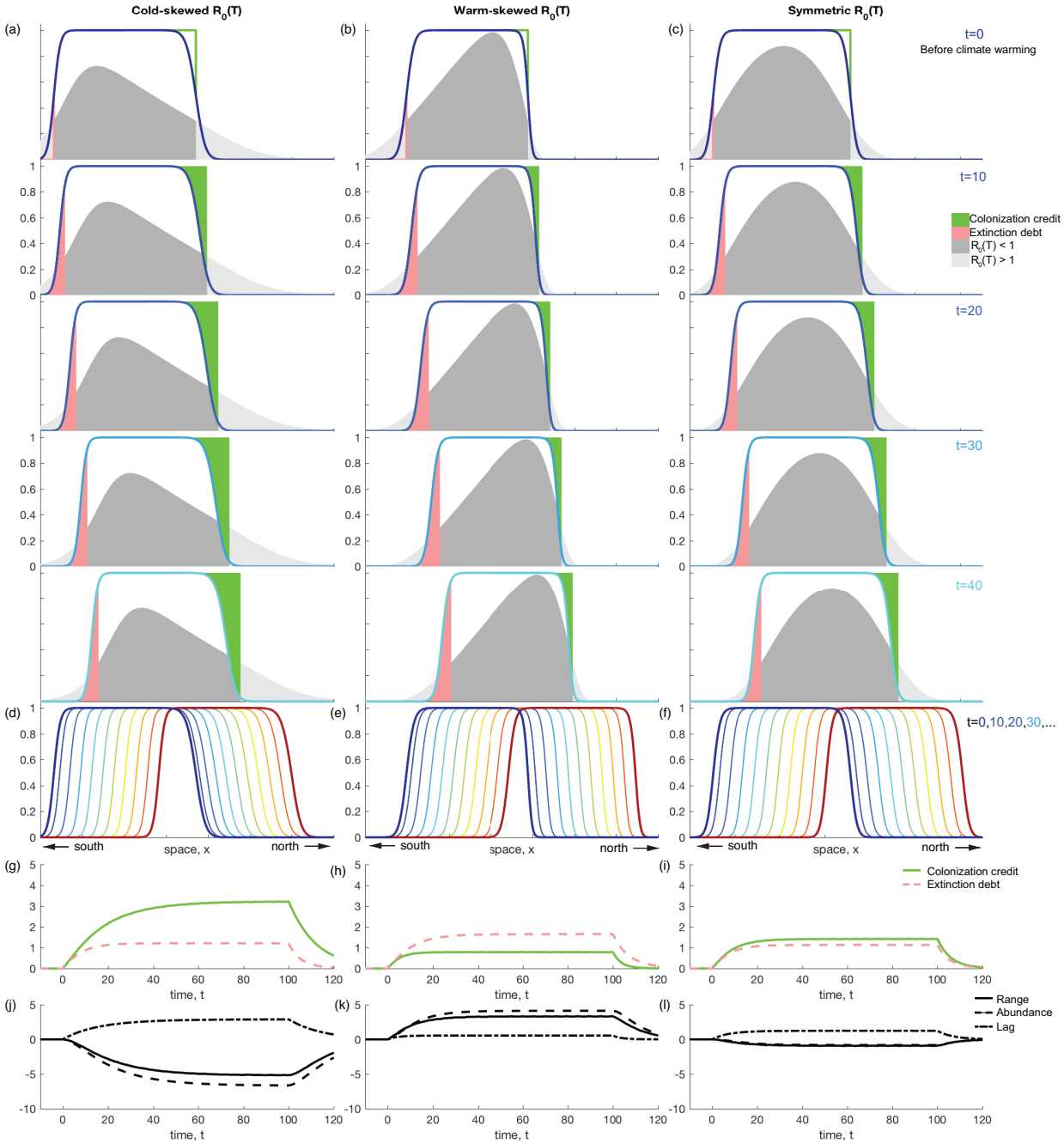

Figure 3. Range change dynamics of species with cold-skewed, warm-skewed and symmetric $R_0(T)$ curves. (a-c) At t=0, climate warming simulations of +0.1°C per year begin, causing the $R_0(T)$ curve to shift northwards (shaded grey, with regions where $R_0(T)$>1 shown darker). Blue curves show the population density responding to this niche shift. Extinction debt (temporary population persistence in regions where $R_0(T)$<1) is shown in shaded pink and colonization credit (population temporarily below carrying capacity despite $R_0(T)$>1) is shown in shaded green. Panels (d-f) show the population density at 10-year increments while climate warming is occurring. Populations with cold-skewed and symmetric $R_0(T)$ have colonization credits that

exceed extinction debt (pink dashed; panels g and i) and thus reduced range size and abundance under climate warming (panels j and l), but the opposite is true for populations with a warm-skewed $R_0(T)$ (panels h and k). Parameter values are as outlined in the main text, with the activation energies E_ρ and E_μ fixed as E_ρ=0.65 eV and E_μ=0 eV (cold-skewed $R_0(T)$), E_ρ=0 eV and E_μ=0.65 eV (warm-skewed $R_0(T)$), and E_ρ= E_μ=0.65 eV (symmetric $R_0(T)$), respectively. To enable visual comparison between a population's $R_0(T)$ and its density, panels (a-c) show $R_0(T)$ multiplied by 0.3.

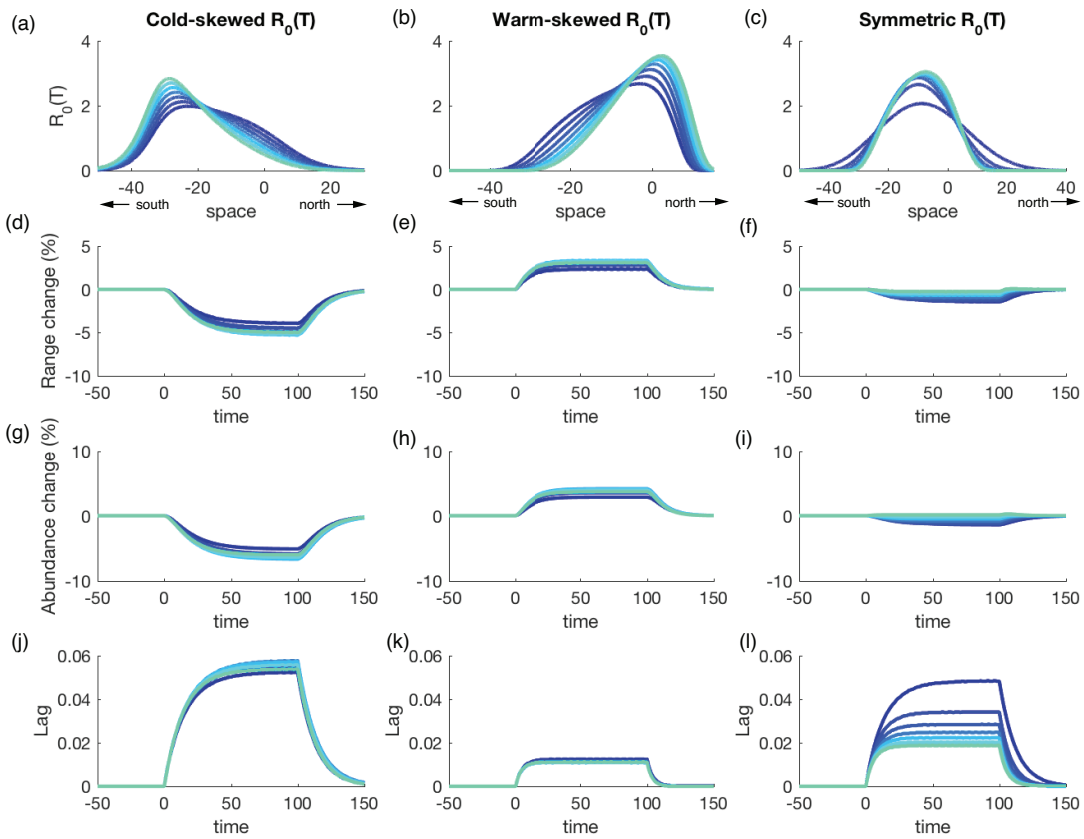

Figure 4. Climate warming adversely affects populations with a cold-skewed $R_0(T)$ (left column), benefits populations with warmed-skewed $R_0(T)$ (middle column), and has relatively little effect on populations with symmetric $R_0(T)$ (right column). (a-c) Different degrees of $R_0(T)$ skewness are explored for each of the cold-skewed, warm-skewed, and symmetric scenarios by varying E_ρ and/or E_μ from 0.2 to 1.1 eV by increments of 0.15 eV (dark to light blue) (all other parameter values are as described in the main text). (d-l) Changes in range size, abundance, and lag before (t<0), during (t=0 to t=100), and after (t>100) warming. The vertical axes in (b-i) are percentage changes relative to the initial range and abundance and in (j-l) are the absolute difference between future lags (t>0) and the lag at time t=0 (cf. SOM Section 3 for details).

Supplementary Material:

Skewed temperature dependence affects range and abundance in a warming world

Amy Hurford, Christina Cobbold, Péter Molnár

Contents

1 Additional simulation details and parameter values **2**
1.1 Simulation details 2
1.2 Parameter values 2

2 Standardization of the results **3**
2.1 How we standardize comparisons between fitness curves with different skewness . 3
2.2 Differences in the initial range size and initial abundance cannot explain the observed impact of climate change 3

3 Effect of mean dispersal distance **6**
3.1 Colonization credit and extinction debt 6
3.2 Final range size, final abundance, and final lag 7

4 Simulations using the Ricker growth function **9**
4.1 Population cycles 12

5 Simulations using the Cauchy dispersal kernel **13**

1 Additional simulation details and parameter values

The main text provides a general overview describing the simulation of our moving-habitat integrodifference equation model with spatially non-uniform net reproduction (equations 1-7). Additional specific details are provided in this section and the MATLAB code used to generate all simulations is archived at Figshare [1] (doi: 10.6084/m9.figshare.6955370).

1.1 Simulation details

Temperature is modelled as a linear gradient along the spatial domain $[-L, L]$ that peaks at $y = -L$, and warming is simulated by increasing temperatures at all locations at a constant rate:

$$T(y,t) = \frac{T_{min,0} - T_{max,0}}{2L} y + \frac{T_{min,0} + T_{max,0}}{2} + wt \tag{S.1}$$

where $T_{max,0}$ and $T_{min,0}$ are the respective temperatures at the southern ($y = -L$) and northern ($y = L$) limits of the spatial domain at time 0, and w is the rate of temperature increase. For simplicity, we ignored seasonal temperature fluctuations in all simulations, assuming a constant T within each year (Figure 1a).

We used computer simulations to explore the range change dynamics given by equations 1-7 in the main text. To do this, we set the initial abundance to 1 on a small interval about $x = 0$, and calculate population densities across the entire spatial domain for 400 years with no change in climate ($w = 0$) to let the population density equilibrate before the onset of warming. Subsequently, we increase the temperature at all locations by $w = 0.1°\text{C yr}^{-1}$ up until an increase of 10°C is achieved after 100 years, and evaluate how warming alters a population's range and abundance, as well as the lag between the northern boundary of the population range and of its thermal niche. We recognize that a warming of 10°C is far more than expected under current climate change predictions, but note that this value was simply chosen to allow easy visualization of how climate change impacts range, abundance, and lag. All results are qualitatively insensitive to the total amount of warming imposed.

To evaluate how the shape of the temperature-dependent fitness curve $R_0(T)$ (equation 4) influences the range change dynamics, we establish cold-skewed, warm-skewed, and symmetric $R_0(T)$ curves by assuming temperature sensitivities in fecundity only, mortality only, or both (cf. also ref. [2]). The strongest cold-skew in $R_0(T)$ arises in populations with highly temperature-dependent fecundity (large E_ρ), but temperature-independent mortality ($E_\mu = 0$). A strongly temperature-dependent mortality (large E_μ) combined with temperature-independent fecundity ($E_\rho = 0$), by contrast, leads to a strongly warm-skewed $R_0(T)$, and equal temperature sensitivities ($E_\rho = E_\mu$) yield an approximately symmetric $R_0(T)$ (Figure 2). We present simulations for these three extreme cases and note that they generate a wide variety of $R_0(T)$ shapes that bound other, more common, combinations of E_ρ and E_μ (Figure 4; i.e. $E_\rho \neq E_\mu$ but both > 0).

1.2 Parameter values

The three cases of cold-skewed, warm-skewed, and symmetric $R_0(T)$ are thus implemented by considering temperature dependence in (i) fecundity only ($E_\rho > 0$, E_μ=0), (ii) survival only ($E_\rho = 0$, $E_\mu > 0$), and (iii) both in fecundity and survival ($E_\rho = E_\mu > 0$). The magnitude of the skew is further manipulated in each of these cases by considering a biologically plausible range of activation energies [3] ($0.2 \leq E_\rho, E_\mu \leq 1.1$), and by setting the inactivation energies such that they further accentuate the direction of any skew in $R_0(T)$ whilst ensuring that the

fundamental niche is contained within the spatial domain (case (i): $E_\rho^L = 3, E_\rho^H = 6$; case (ii): $E_\mu^L = 6, E_\mu^H = 3$; case (iii): $E_\rho^L = E_\rho^H = E_\mu^L = E_\mu^H = 5E_\rho = 5E_\mu$; Figure 4). The remaining model parameters were fixed arbitrarily, but chosen such that dispersal is large enough that the population can keep pace with its moving niche ($D = 0.5, K = 1$, μ_0=-ln(0.2), $\rho_0 = 50$, $T_\rho^L = T_\mu^L$ =5°C, $T_\rho^H = T_\mu^H$ =20°C , $T_0 = 12.5$°C, $T_{min,0} = -15°C$, $T_{max,0} = 30°C$; note that all temperatures are reported in °C for simplicity but converted to Kelvin for use in equations 5-8). Finally, we standardized each fitness curve so that the total reproductive potential of an organism across the entire landscape is always a constant (chosen as $\bar{R} = 75 = c_1 \int_{-L}^{L} R_0(x)\, dx$ where c_1 is the calibration parameter). This calibration ensures that the shape of $R_0(T)$ is the main source of variation in all comparisons, and that qualitative differences in climate change impacts can therefore be attributed to differences in this fitness curve shape (see Section 2). While the values of ρ_0, μ_0, T_L, T_H and $\bar{R}$ were chosen arbitrarily, our results are not sensitive to these choices because it is the shape of the fitness curve, rather than the specific details of how the curves are produced, that determines the impact of climate warming.

2 Standardization of the results

2.1 How we standardize comparisons between fitness curves with different skewness

Throughout this study, we quantify the impacts of climate warming by comparing range size, abundance, and lag relative to their initial values. The range change (%) is calculated by taking the range size at time t divided by the initial range size (when climate warming begins at $t = 0$) and multiplied by 100, and the abundance change (%) is calculated in the same way. The lag is calculated by subtracting the lag at time $t = 0$ from the lag at time t. Final range size, final abundance, and final lag are calculated as described above, but with $t = 100$ (the time when climate warming ends). In addition, we normalized all fitness curves so that the reproductive potential of a population (the integral of $R_0(T)$ across all of space) is equal to the same value ($\bar{R}$) regardless of fitness curve skew. This normalization was necessary to ensure that results reflect differences in fitness curve skewness and are not due to associated changes in reproductive potential.

2.2 Differences in the initial range size and initial abundance cannot explain the observed impact of climate change

The normalization of the reproductive potential for all fitness curves to $\bar{R}$ does not ensure that the initial range sizes, initial abundances, or initial lags are also equal for different $R_0(T)$ (Table S.1) because these quantities are also influenced by density-dependent processes that are not captured by $R_0(T)$, which describes only the net reproduction at low densities (see equation 3 in the main text). In Figure S.1, we demonstrate that differences in initial range size and initial abundance between different $R_0(T)$ curves cannot explain the systematic climate change impact differences, which are instead driven by the differences in fitness curve skewness. To interpret Figure S.1, note that fitness curves with cold-skew ($*$), warm-skew ($\triangle$), and symmetric ($\bullet$) shapes may all have initial range sizes close to 41 (left column), but the initial range size of 41 corresponds to a wide range of final range sizes (between -6 and +2% change), whereas cold-skewed curves ($*$), of any initial range size, correspond to a narrower range of final range sizes (between +2 and +4% change; Figure S.1a). This pattern is generally consistent for different initial abundances (right column), and if different climate warming impacts are considered

color	E_{par}	cold-skewed			warm-skewed			symmetric		
		init. range	init. abund.	init. lag	init. range	init. abund.	init. lag	init. range	init. abund.	init. lag
Navy blue	0.2	47.99	37.43	-0.087	40.61	32.71	-0.043	47.04	35.53	-0.085
Dark blue	0.35	46.93	36.30	-0.089	39.26	31.35	-0.042	41.73	32.02	-0.072
Royal blue	0.5	45.75	35.06	-0.091	37.99	30.08	-0.041	39.65	30.73	-0.066
Baby blue	0.65	44.50	33.78	-0.092	36.88	29.02	-0.041	38.76	30.32	-0.062
Aqua	0.8	43.27	32.56	-0.092	36.02	28.21	-0.041	38.23	30.13	-0.058
Turquoise	0.95	42.10	31.43	-0.091	35.39	27.64	-0.041	37.79	29.91	-0.056
Bright mint	1.1	41.03	30.44	-0.090	34.98	27.28	-0.041	37.29	29.57	-0.053

Table S.1: The initial range size, initial abundance, and initial lag for all the fitness curves considered in Figure 4 of the main text. All fitness curves are normalized so that the reproductive potential (the integral of $R_0(T)$ across all of space) is the same regardless of fitness curve skew, but this does not lead to equal initial range sizes, initial abundances and initial lags. E_{par} is the parameter that is manipulated to adjust the strength of the skew: $E_{par} = E_\rho$ (cold-skewed), $E_{par} = E_\mu$ (warm-skewed), and $E_{par} = E_\rho = E_\mu$ (symmetric). Negative values of the lag mean that the population density is above the detection threshold and the population is persisting in a region ahead of the thermal tolerance limits described by the fundamental niche. As discussed in the main text, this is due to a continuous space analog of the familiar source-sink dynamics described for discrete space patch-based metapopulation models [4], whereby a population outside the fundamental niche is sustained through dispersal.

(rows), and so we conclude that differences in initial range size or initial abundance are not responsible for the different climate warming impacts that we observe.

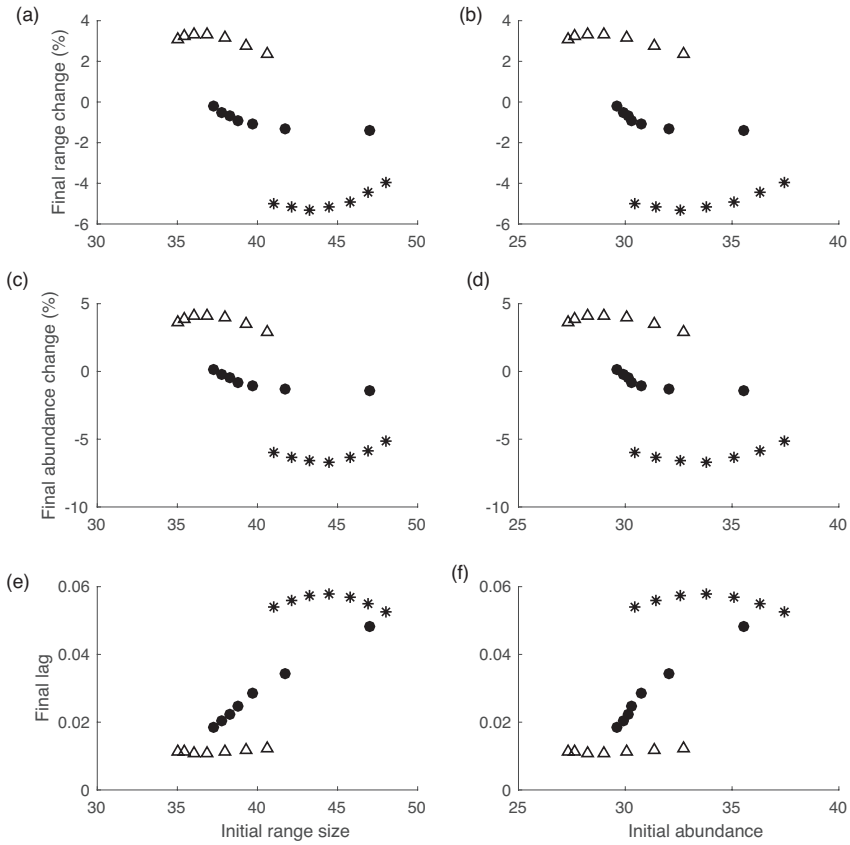

Figure S.1: Initial range size (left column) and initial abundance (right column) do not have a strong effect on how warming impacts final range size (top row), final abundance (middle row) and final lag (bottom row). In contrast, there is a strong relationship between the skewness of $R_0(T)$ and the effects of climate warming (symbols: cold-skewed - $*$, warm-skewed - $\triangle$, symmetric - $\bullet$).

3 Effect of mean dispersal distance

In this section, we analyze how mean dispersal distance affects a population's colonization credits, extinction debts, range size, abundance, and lag during range changes.

3.1 Colonization credit and extinction debt

Colonization credit occurs in locations where the population is below its carrying capacity despite $R_0(T) > 1$, and is quantified as the difference between the carrying capacity and the population density numerically integrated across locations meeting these criteria. Colonization credit quantifies the additional abundance the environment could support, if it were not for dispersal limitation. In contrast, extinction debt occurs in areas where the population remains temporarily present despite $R_0(T) < 1$, and is defined as the numerical integral of the population density across all these locations. Extinction debt is thus the abundance of this population that can only persist temporarily (see Figure 1 in the main text).

Figure S.2 shows that both colonization credits and extinction debts decrease as the mean dispersal distance. The decrease in colonization credit as the mean dispersal distance increases (Figure S.2, green solid lines) is since a larger proportion of offspring disperse longer distances from their natal sites, and are thus better able to colonize new habitat and keep pace with their moving fundamental niche. There are two factors that explain why extinction debt decreases with increasing mean dispersal distance (Figure S.2, pink dashed lines). Firstly, the population is better able to track the location of the fundamental niche with larger dispersal distances, meaning that fewer individuals begin their dispersal from a position behind the trailing edge of the niche, resulting in smaller extinction debts. Secondly, any group of individuals that does start behind the trailing edge, with larger dispersal distances, will see a larger proportion of dispersers catching up with the niche, again lessening the extinction debt. Despite both colonization credit and extinction debt decreasing with mean dispersal distance, populations with cold-skewed fitness curves remain more adversely affected by climate warming (Figure S.22a) in comparison to their warm-skewed counterparts (Figure S.2b) for all choices of mean dispersal distance (Figure S3). Figure S.2 shows that if colonization credit is greater than extinction debt, then this holds for all values of the mean dispersal distance (and visa versa), which in turn implies that abundance changes for fitness curves of a given skewness are robust to different mean dispersal distances.

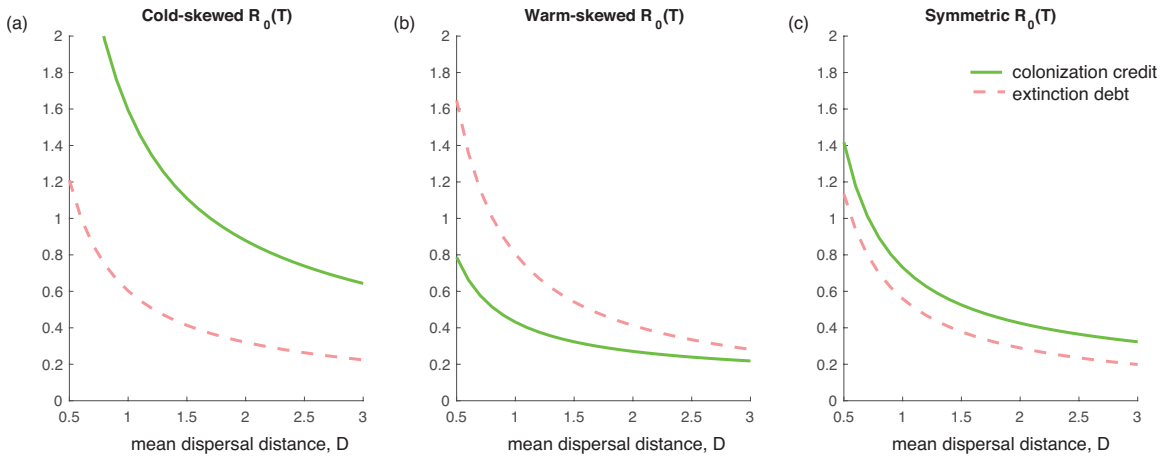

Figure S.2: As the mean dispersal distance increases, colonization credits and extinction debts (after 100 years of climate warming) decrease. Simulation parameters are the same as for Figure 4 of the main text, except that the mean dispersal distance varied as indicated on the x-axis.

3.2 Final range size, final abundance, and final lag

Populations are better able to keep pace with climate change as mean dispersal distance (D) increases, resulting in smaller lags, and larger final range sizes and final abundances (Figure S.3). Our qualitative results from the main text remain unchanged for different choices of mean dispersal distance (Figure S.3): climate warming results in range size and abundance decreases for organisms with cold-skewed fitness curves and in range size and abundance increases for organisms with warm-skewed fitness curves (Figure S.3). Mean dispersal distances smaller than 0.5 were not considered in our simulations as the population with the cold-skewed fitness curve fails to keep pace with climate change in these cases.

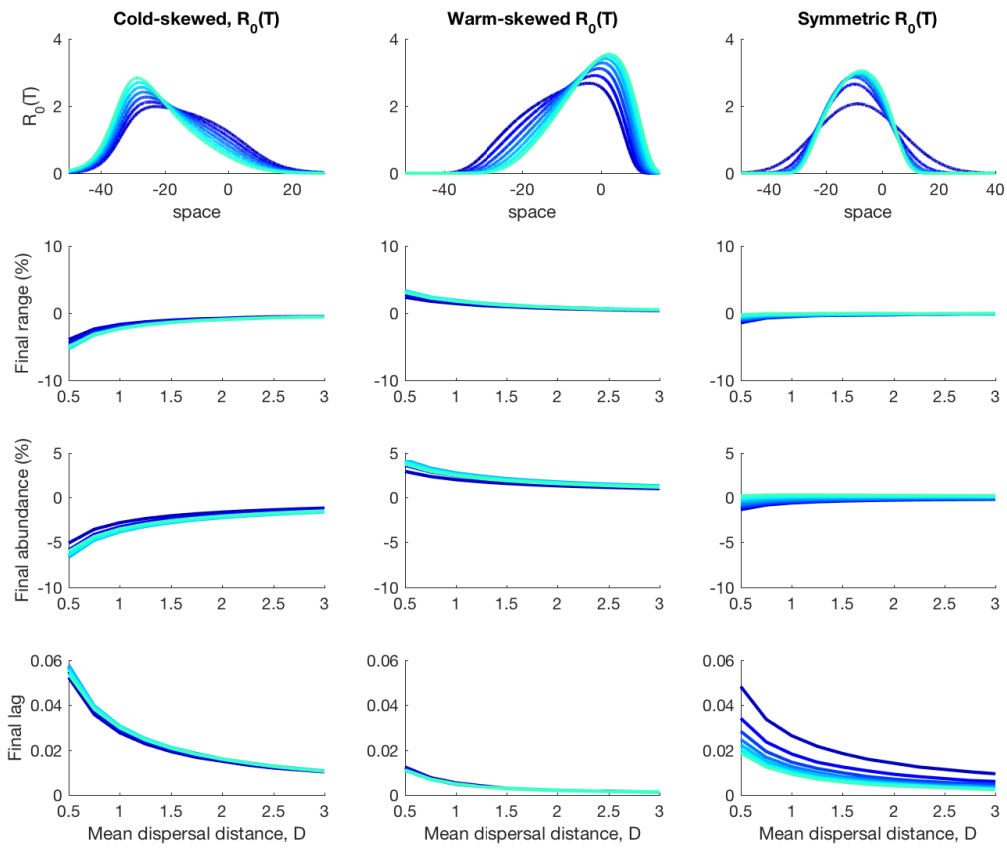

Figure S.3: The impacts of climate warming are qualitatively insensitive to changes in the mean dispersal distance in the Laplace dispersal kernel: a larger mean dispersal distance lessens the impacts of warming, but the direction of change is maintained for all cases of $R_0(T)$ skewness. Parameters are identical as in Figure 4 of the main text, but in this figure only the final range size, final abundance and final lag (at $t = 100$) are shown.

4 Simulations using the Ricker growth function

In the main text, we evaluated range change dynamics for the case of compensatory density dependence using a Beverton-Holt population growth model (equation 3). Here, we assess whether results differ for overcompensatory density dependence using the Ricker model for population growth. The Ricker growth function is given by,

$$f(n_t(y), T(y,t)) = n_t(y) \exp\left(r(T(y,t)) - \frac{r(T(y,t))n_t(y)}{K}\right), \tag{S.2}$$

where $r(T(t,y)) = \ln(R_0(T(y,t)))$ and K is the carrying capacity. As in the Beverton-Holt scenario, this carrying capacity is independent of R_0, as can be seen from rewriting equation S.2 as,

$$f(n_t(y), T(y,t)) = \begin{cases} R_0(T(y,t))\ n_t(y)\ \exp\left(-\frac{\ln(R_0(T(y,t)))\ n_t(y)}{K}\right), & \text{for } R_0(T(y,t)) > 0, \\ 0, & \text{for } R_0(T(y,t)) = 0. \end{cases} \tag{S.3}$$

Combining the Ricker growth function with the Laplace dispersal kernel yields near identical values for our summary statistics as in the Beverton-Holt/Laplace scenario (Figures S.4 and S.5). The only exception is for large values of $R_0(T)$ as discussed in the next section.

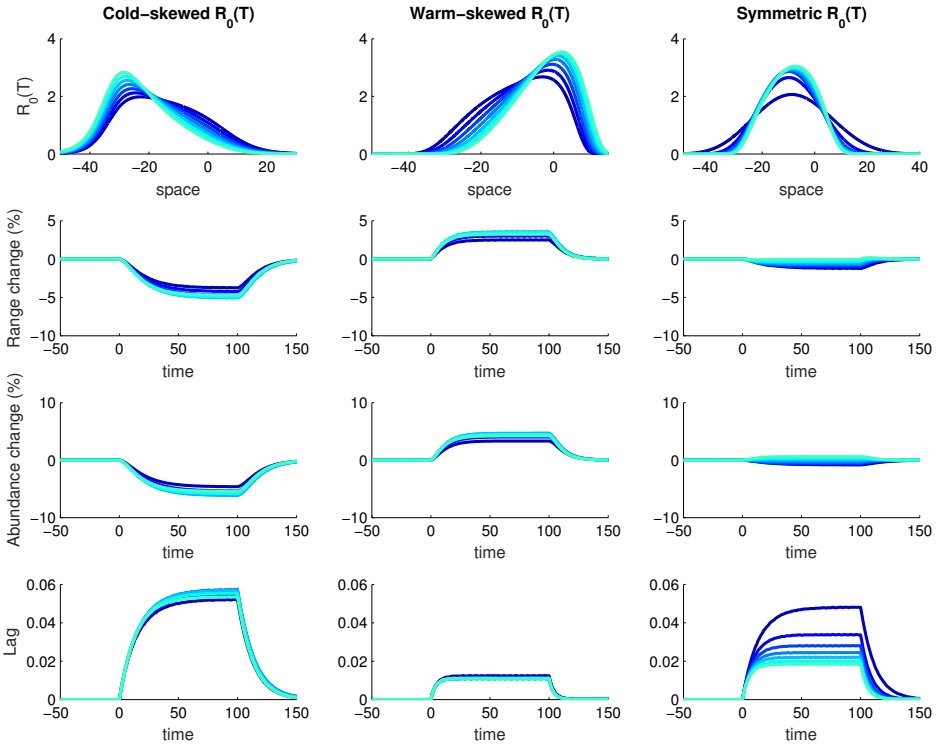

Figure S.4: Analogous to Figure 4 in the main text, but now using the Ricker population growth model instead of the Beverton-Holt model.

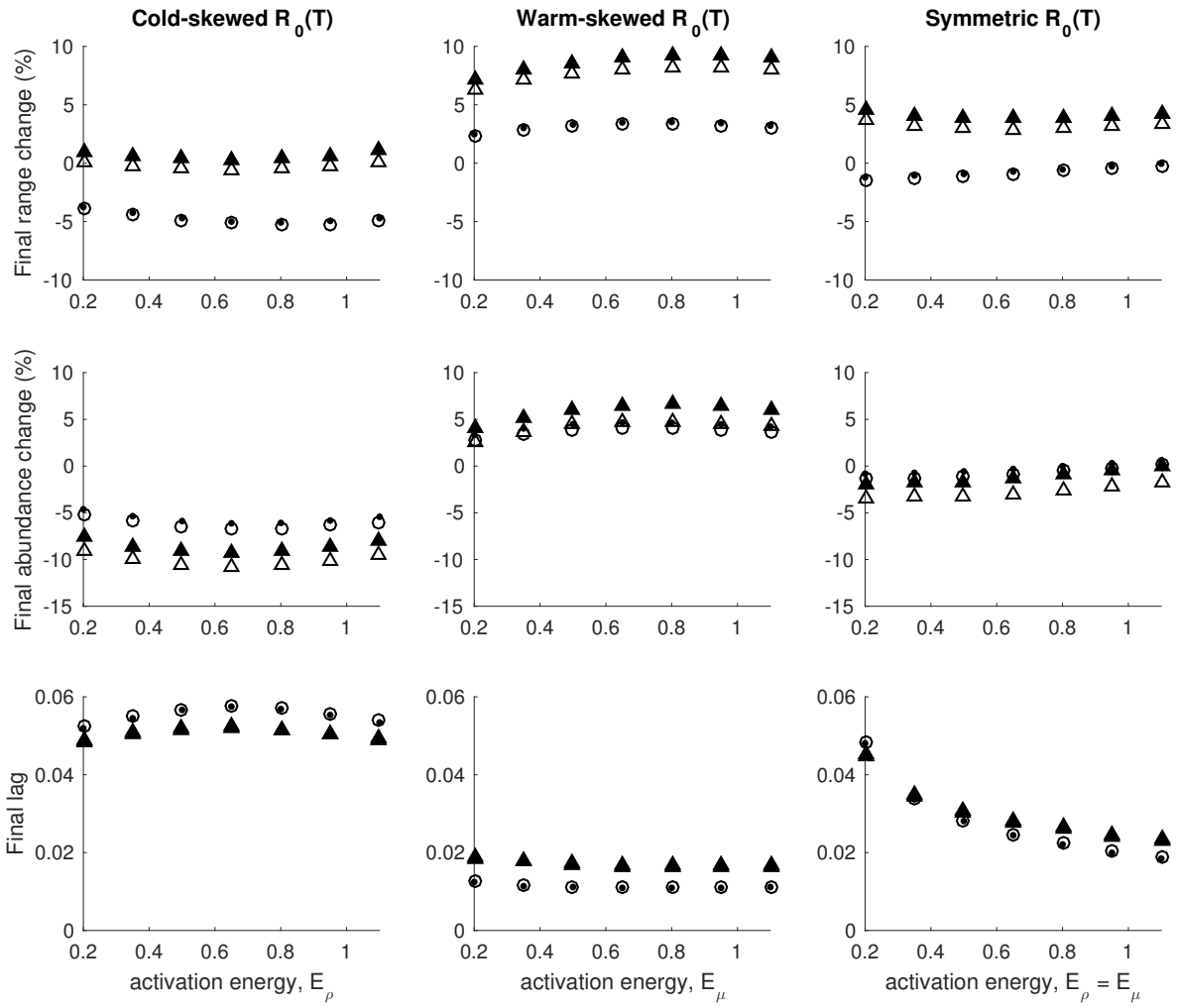

Figure S.5: The effect of $R_0(T)$ skewness on a population's response to climate warming is similar for different combinations of Beverton-Holt or Ricker population growth models and Laplace or Cauchy dispersal kernels. The final range size (top row), final abundance (middle row) and final lag (bottom row) after 100 years of climate warming are shown for the Beverton-Holt/Laplace (○), Ricker/Laplace (·), Beverton-Holt/Cauchy (△), and Ricker/Cauchy (▲) combinations of population growth models and dispersal kernels. In each of these scenarios, populations with cold-skewed $R_0(T)$ are adversely impacted by climate warming, warm-skewed $R_0(T)$ benefit from climate warming, and symmetric $R_0(T)$ are unaffected or experience mixed responses. Simulation parameters are as in Figure 4 in the main text and $\beta = 0.005$ was used in the Cauchy dispersal kernel.

4.1 Population cycles

Climate change may dampen or eliminate population cycles. For large values of $R_0(T)$, prior to climate change the Ricker population growth function gives rise to a two-cycle in population density (Figure S.6a), but when climate warming occurs the population cycles dampen (Figure S.6b,d). After the end of climate warming, the population density returns to an identical two-cycle pattern, but displaced northwards due to the warming-induced northern shift in the fundamental niche.

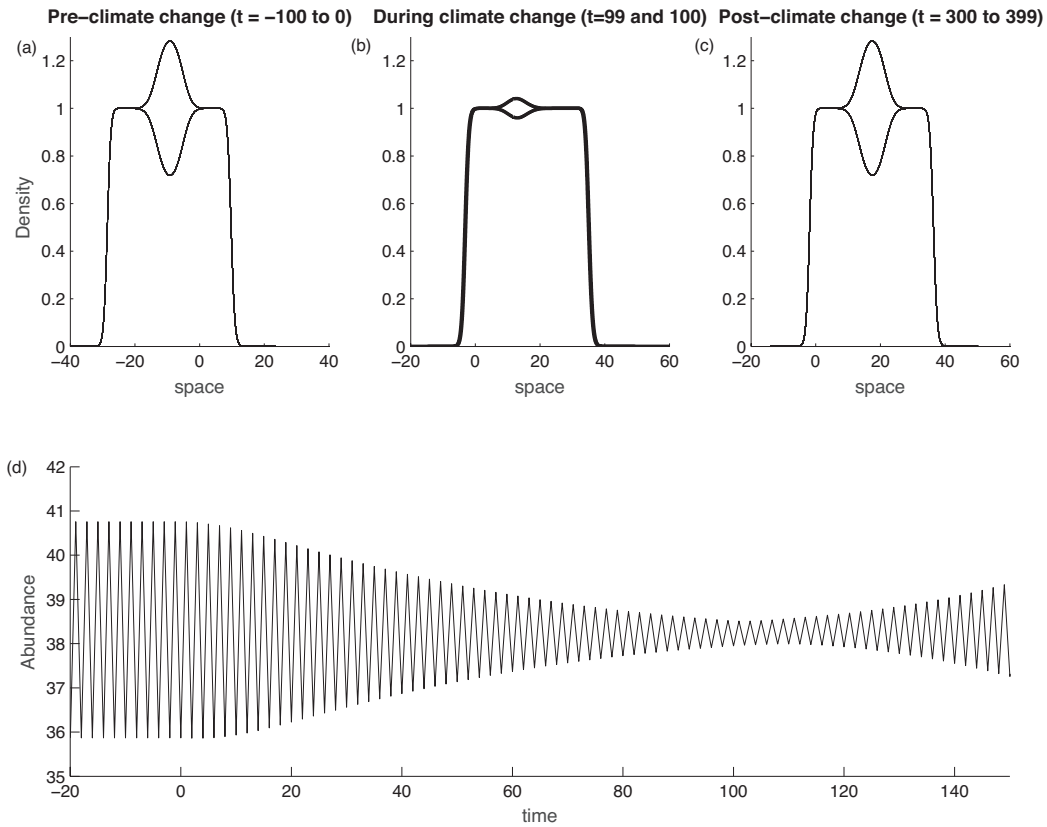

Figure S.6: Climate warming may dampen population cycles arising from overcompensation. (a) For Ricker population growth, prior to climate warming the population exhibits a stable two-cycle (the population density is shown every year for 100 years prior to the onset of climate warming from t=-100 to 0). (b) The population cycles are dampened during climate warming and the abundance becomes less variable (d). (c) After climate warming ends the population converges back to the original stable two-cycle, but displaced northwards. The parameters are $D = 0.5$, $\bar{R} = 1$, ρ_0=44 with all other parameters as in Figure 4 of the main text.

5 Simulations using the Cauchy dispersal kernel

In the main text, we evaluated range change dynamics for the case of an exponentially bounded (Laplace) dispersal kernel. Here, we assess whether results differ for a fat-tailed dispersal kernel (Cauchy) because population spread rates are known to be greatly influenced by the tail of the kernel [5]. The Cauchy kernel is commonly used to model 'fat-tailed' dispersal and is given by,

$$k(x-y) = \frac{\beta}{\pi(\beta^2 + (x-y)^2)}, \tag{S.4}$$

where β is a shape parameter. Compared to the Laplace distribution, which exhibits exponential decay in the tail of the distribution, the Cauchy distribution is 'fat-tailed' due to the power law decay of the tail. The associated higher number of long-distance dispersal events explains both why range sizes are larger under a Cauchy kernel and why abundances are smaller (more individuals are lost due to long-distance dispersal into hostile habitat; Figure S.5). Nevertheless, with the Cauchy dispersal kernel our general result remains: climate warming will adversely affect populations with cold-skewed fitness curves (substantially decreasing abundance), benefit populations with warm-skewed fitness curves, and will have mixed effects on populations with symmetric fitness curves.

Simulations that use the Cauchy dispersal kernel were run with $\beta = 0.005$, where 2β is the width of the distribution at half its maximum (for reference, the corresponding width for the Laplace distribution is $2D \ln 2$, where D is the mean dispersal distance). Figure S.7 is analogous to Figure 4 of the main text except that the Cauchy dispersal kernel is used. Ricker population growth combined with a Cauchy dispersal kernel yields near identical results to the combination of the Beverton-Holt growth function with the Cauchy dispersal kernel (Figure S.5, triangle symbols).

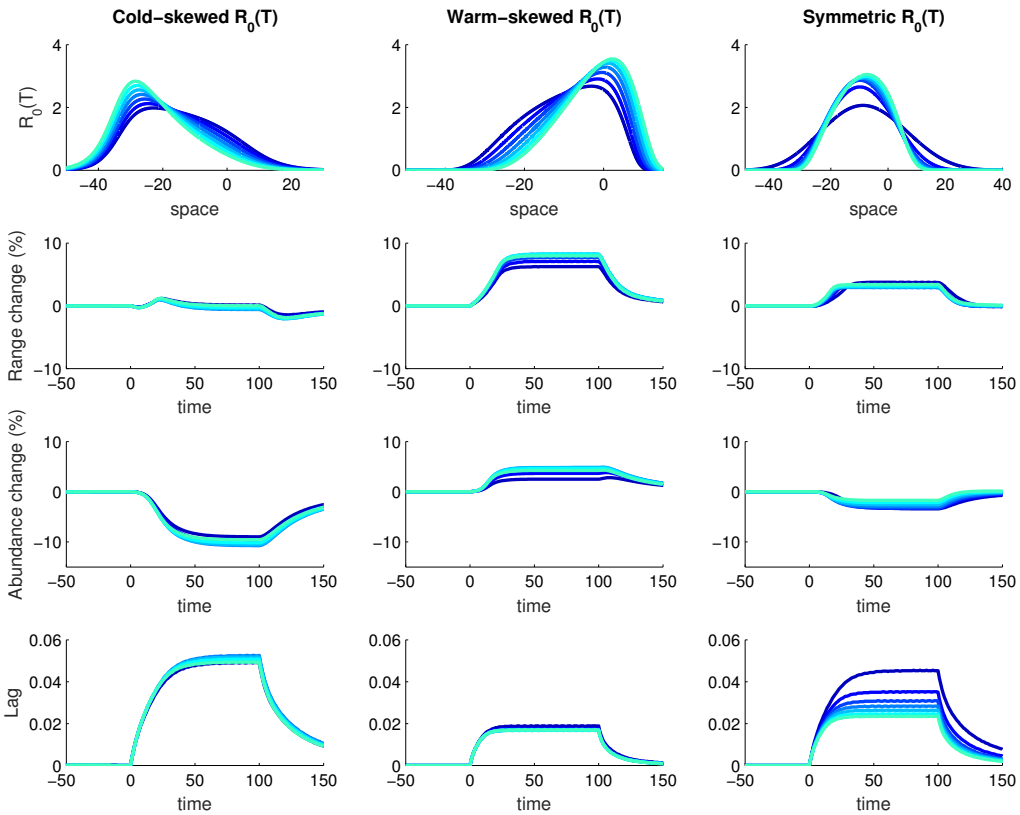

Figure S.7: This figure is analogous to Figure 4 in the main text except that the Cauchy dispersal kernel replaces the Laplace dispersal kernel from Figure 4. In contrast to the results found for the Laplace dispersal kernel, for the Cauchy dispersal kernel we observe: 1) larger range sizes, and 2) smaller abundances during climate change. For this figure $\beta = 0.005$ and all other parameters are identical to Figure 4.

References

[1] Hurford, A., C. Cobbold, and P. K. Molnár. 2018. Skewed temperature dependence affects range and abundance in a warming world (Code). *Figshare* doi: 10.6084/m9.figshare.6955370.

[2] Molnár, P. K., Kutz, S. J., Hoar, B. M. and Dobson, A. P. 2013. Metabolic approaches to understanding climate change impacts on seasonal host-macroparasite dynamics. *Ecology Letters* 16, 9?21.

[3] Dell, A. I., Pawar, S. and Savage, V. M. 2011. Systematic variation in the temperature dependence of physiological and ecological traits. *Proceedings of the National Academy of Sciences* 108, 10591?10596.

[4] Pulliam, R.H. 1988. Sources, sinks, and population regulation. *The American Naturalist* **132**: 652-661.

[5] Zhou, Y. and M. Kot. 2013. Life on the Move: Modeling the Effects of Climate-Driven Range Shifts with Integrodifference Equations in Dispersal, Individual Movement and Spatial Ecology (Lewis, M.A., Maini, P.K. and S.V. Petrovskii, Eds.). Springer, Berlin, Heidelberg.